Available online at www.sciencedirect.com
SCIENCE DIRECT®
Journal of Nuclear Materials 353 (2006) 109–118
journal of nuclear materials
www.elsevier.com/locate/jnucmat

# Creep fracture of zirconium alloys

Troy A. Hayes [a,*], Robert S. Rosen [b], Michael E. Kassner [c]

[a] Exponent Failure Analysis Associates, 149 Commonwealth Drive, Menlo Park, CA 94025, USA
[b] Defense Nuclear Facilities Safety Board, 625 Indiana Avenue, NW, Suite 700, Washington, DC 20004, USA
[c] University of Southern California, Aerospace and Mechanical Engineering Department, Olin Hall 430, Los Angeles, CA 90089, USA

Received 13 October 2005; accepted 17 February 2006

**Abstract**

Theoretical approaches utilized to predict the lifetime of spent nuclear fuel in interim dry storage assumed that diffusion controlled cavity growth controlled the failure time under these conditions. DCCG, however, fails to account for the fact that the failure time is related to the strain rate in Zircaloys according to the Monkman–Grant relationship. This paper will show that constrained cavity growth, which can account for the Monkman–Grant relationship but was not considered in the spent nuclear fuel lifetime prediction models, is more relevant to failure of spent nuclear fuel in dry storage. Contrary to reports in the past, constant stress creep tests performed in this study on Zircaloy-2 suggest that creep cavity nucleation and/or growth occurs prior to tertiary creep. Constant strain rate creep rupture tests on Zircaloy-2 show strong evidence of extensive cavity nucleation and growth near and at the fracture surface, indicating a creep cavitation failure mechanism under these conditions.


## 1. Introduction

Upon removal from reactor, spent nuclear fuel (SNF) rods are placed in wet storage for a period of generally 5 years or more. The wet storage capacity at commercial nuclear power plants is inadequate to accommodate all the SNF until a permanent disposal site becomes available. This has led to the development of interim dry storage, where SNF rods are placed inside a canister, usually concrete with a stainless steel liner, in air or an inert atmosphere while awaiting permanent disposal. An increasing number of rods are now being placed in interim dry storage due to delays in the availability of a permanent disposal site (mined geologic repository). Commercial SNF typically consists of uranium dioxide pellets surrounded by a thin cladding, usually a zirconium-based alloy such as Zircaloy-2 or Zircaloy-4. The Nuclear Regulatory Commission (NRC) formerly required potential dry storage licensees to calculate the maximum allowable temperature for the storage of spent nuclear fuel based on creep rupture models [1]. The NRC then accepted calculations based on a strain-limit approach as an alternative for the model-based calculations [2]. The NRC subsequently abandoned all 'creep theoretical' models, as well as the strain-limit approach, in favor

* Corresponding author. Tel.: +1 650 688 7127.
*E-mail address:* thayes@exponent.com (T.A. Hayes).

0022-3115/$ - see front matter © 2006 Elsevier B.V. All rights reserved.
doi:10.1016/j.jnucmat.2006.02.093

of temperature limits that are based on an examination of spent fuel rods after 15 years of dry storage [3,4].

There is a belief in the nuclear industry that zirconium alloys are resistant to void formation and that creep cavitation plays little or no role in the creep failure of these alloys [5,6], contrary to the results of a study by Keusseyan et al. [7]. The objectives of this study were to evaluate the relevant failure mechanisms for zirconium alloys under SNF interim dry storage conditions and to determine whether creep cavity nucleation and growth occur in Zircaloy-2 under these conditions. A creep theoretical evaluation, constant strain rate creep fracture tests, and constant stress creep tests were employed to meet these objectives.

## 2. Creep fracture model

Zircaloy cladding in interim dry storage is subjected to stresses up to approximately 100 MPa and temperatures as high as 450 °C. It has been suggested that a failure mechanism known as diffusion-controlled cavity growth (DCCG) as originally proposed by Hull and Rimmer [8], and later modified by Raj and Ashby [9] and Speight and Beere [10], controls the failure of zirconium alloys under these conditions [11,12]. The rupture time according to this model is given by [19]

$$t_f = \frac{3\pi^{1/2}}{32}\frac{F_v(\alpha)}{F_B(\alpha)^{3/2}}\int_{A_{min}}^{A_{max}}\frac{dA}{f(A)}\frac{\lambda^3 kT}{\Omega D_{gb}\delta\sigma}, \quad (1)$$

where $t_f$ is the fracture time, $F_v$ and $F_B$ are functions of the grain boundary/cavity interfacial angle, $\alpha$, $A$ is the area fraction of grain boundaries occupied by cavities, $k$ is Boltzman's constant, $T$ is temperature, $\Omega$ is the atomic volume, $D_{gb}$ is the grain boundary diffusion coefficient, $\delta$ is the grain boundary width, $\sigma$ is the applied stress and $\lambda$ is the average cavity spacing. Although this model has been shown to be applicable under very limited conditions (see, for example, Refs. [13–16]), it does not appear to apply to many engineering materials because, as is apparent in Eq. (1), the failure time according to this model is not a function of the strain rate. It is known, however, that the failure time in many engineering metals and alloys (including Zircaloy-2 [17]) is related to the strain rate by the Monkman–Grant relationship, or

$$\dot{\varepsilon}_{ss} t_f = K, \quad (2)$$

where $K$ is the Monkman–Grant constant, $t_f$ is the fracture time, and $\dot{\varepsilon}_{ss}$ is the steady-state strain rate. Thus, pure, or 'unconstrained' DCCG may not be applicable to zirconium alloys. Strain-based creep cavitation models, however, do not appear to be able to account for the magnitude of cavity growth observed in practice. Instead, a constrained cavity growth model, which can lead to significant cavity growth without large far-field strains and can account for the Monkman–Grant relationship, may be the most relevant for predicting the lifetime of nuclear fuel rods during interim dry storage. Constrained cavity growth is discussed in detail elsewhere [18]. Briefly, unconstrained cavity growth assumes that every grain boundary that lies nearly perpendicular to the applied stress undergoes uniform cavitation. A more realistic assumption is that the cavitating grain boundaries in a metal are interspersed among many cavity-free grains. As cavity growth proceeds on isolated grain boundaries, the adjacent grains begin to elongate in order to accommodate the local increase in volume created by the grain boundary cavities. The stress driving the growth then becomes 'constrained' by surrounding grains that do not contain cavities and do not, therefore, undergo the same local strain. Once the stress is relieved or 'shed' by the constraint of surrounding grains, cavity growth ceases until the surrounding grains deform and the stress on the cavitated grain boundaries rises again. The time for cavity coalescence to occur was calculated by Reidel [19] to be

$$t_c = 0.004\frac{kT\lambda^3}{\Omega\delta D_{gb}\sigma} + 0.3\frac{(1+3/n)^{1/2}\lambda}{\dot{\varepsilon} g}, \quad (3)$$

where $t_c$ is the time to coalescence, $g$ is the grain size, $\dot{\varepsilon}$ is the strain rate, $n$ is the power law (stress) exponent and the other factors are consistent with Eq. (1), above. The range of conditions under which constrained cavity growth is rate controlling was calculated and compared to the conditions relevant to the interim dry storage of SNF. Fig. 1 indicates the 'constrained limit stress' ($\sigma_c$) below which constrained cavity growth is predicted to control cavity growth and, ultimately, fracture, along with the conditions relevant to the dry storage of SNF.

The time to coalescence was assumed to be 'constrained' when the creep-controlled portion of Eq. (3) (the second term) was approximately equal to the diffusion-controlled portion of Eq. (3) (the first term). As the applied stress is decreased below the

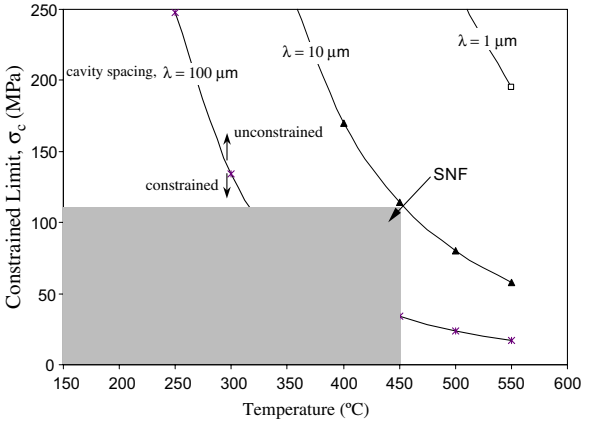


Fig. 1. Constrained cavity growth limit stress as a function of temperature and cavity spacing for Zircaloy-2. The shaded box indicates approximate spent nuclear fuel (SNF) storage conditions.

constrained limit, the constraint has an increasingly large effect on the time to coalescence. As the applied stress is increased above the constrained limit, the unconstrained portion (DCCG portion) of the coalescence time becomes increasingly dominant.

In developing Fig. 1, a typical grain size ($g$) of 8 μm, a grain boundary width ($\delta$) of 0.97 nm, a power-law exponent ($n$) of 4.8 and an atomic volume ($\Omega$) of $3.37\times10^{-29}$ m$^3$ were assumed. The strain rate of the SNF was taken as $10^{24}\exp(-Q_C/\mathrm{RT})\,(\sigma/G)^n$ (s$^{-1}$) based on the average strain rate determined from the cumulative data in the intermediate stress (five-power-law) regime measured from the literature (presented in Fig. 2). The grain boundary diffusion coefficient was assumed to be $5\times10^{-4}\exp(-167$ kJ/mol/RT) m$^2$/s. It is apparent in Fig. 1 that constrained cavity growth is extremely relevant to Zircaloy cladding under SNF storage conditions for all cavity spacings less than approximately 10 μm and for most conditions for cavity spacings less than approximately 100 μm (the cavity spacing assumed by the models formerly utilized by dry storage licensees to calculate the maximum allowable temperature for dry storage of SNF was less than 10 μm).

The 'constrained limit' was calculated based on an instantaneous nucleation assumption (assuming that all grain boundary cavities are present at the time of first stress application). In reality, cavities are likely continuously nucleated with time (strain). Nonetheless, using the instantaneous nucleation assumption yields the most conservative result as

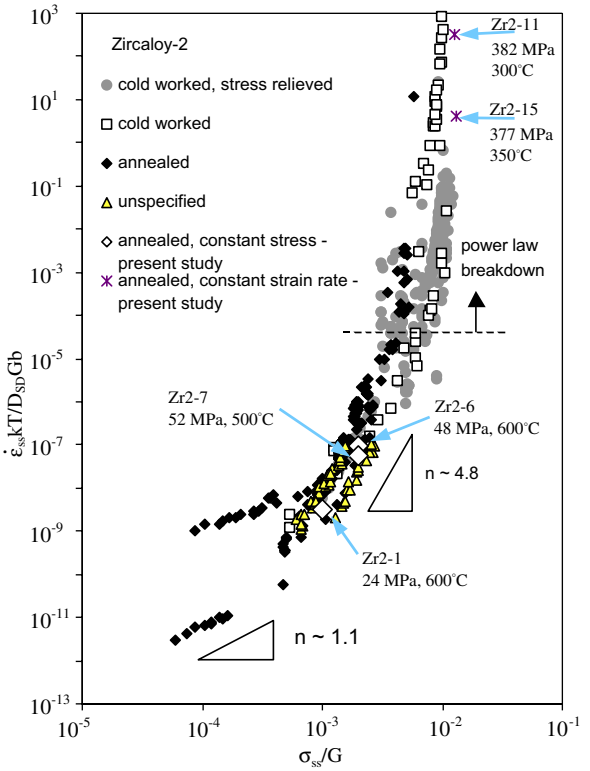


Fig. 2. Diffusion coefficient-compensated steady-state strain rate versus modulus-compensated steady-state stress data for Zircaloy-2 from the literature and the present study (see Ref. [20] for references).

long as the cavity spacing is chosen appropriately. These calculations were also performed under the assumption that the behavior of SNF rods can be conservatively modeled based on unirradiated creep data. This appears to be a valid assumption because irradiated Zircaloy has been shown to have similar or higher creep strength than unirradiated Zircaloy [20]. The constraining effect tends to increase with decreasing strain rates, so constraint may be more relevant to (irradiated) SNF than to unirradiated Zircaloy. In addition, irradiation may cause void nucleation at or near grain boundaries (as will be discussed below). These voids may grow during dry storage and contribute to creep damage accumulation and failure.

The failure time of SNF under dry storage conditions predicted by a constrained cavity growth model is potentially significantly longer than those calculated using an unconstrained model. The details of the differences in predicted failure times under various assumptions are discussed elsewhere [21].

## 3. Creep cavitation in zirconium alloys

It has been reported that Zircaloys are very resistant to neutron radiation induced void formation (e.g. [22–25]), at least under the specific conditions of the respective experiments. Some have suggested theories as to why voids do not form in Zircaloys during irradiation (see [26–28]). More, recently, however, it has been shown that cavities commonly form in zirconium and zirconium alloys under neutron irradiation [29–33]. The voids sometimes nucleate heterogeneously adjacent to defects such as vacancy dislocation loops, which form preferentially near grain boundaries during irradiation [29–31]. Such studies have not been performed on irradiated spent nuclear fuel. Even if such cavities did form in Zircaloy nuclear fuel cladding, it is not clear whether the cavities formed during irradiation would play any roll in creep failure under dry storage conditions.

As discussed above, zirconium alloys appear to obey the Monkman–Grant relationship, similar to many other engineering materials. It has also been shown that the fracture time in Zircaloy-4 can be predicted using the Larson–Miller parameter between temperatures of 365–584 °C and stresses of 64–410 MPa [34,35]. Other materials that obey such relationships often fail as a result of creep cavity growth and coalescence. Thus, it is foreseeable that zirconium alloys may also exhibit such behavior. The relevance of the constrained cavity growth model (or any other cavitation-based failure model) to the dry storage of spent nuclear fuel is predicated on the assumption that zirconium alloys undergo creep cavity nucleation and growth. As discussed above, there is no consensus as to whether zirconium alloys are susceptible to creep cavitation. One of the main objectives of this study, then, was to determine whether zirconium alloys exhibit creep cavity nucleation and growth under conditions relevant to the dry storage of SNF. Another goal of this study was to determine whether creep cavitation plays an important roll in creep fracture in zirconium alloys.

## 4. Experimental procedure

The Zircaloy-2 utilized in this study was obtained in the form of a 16-mm diameter rod from Allegheny Wah Chang in Albany, Oregon. The processing consisted of several heating (at temperatures ranging from 660 to 1110 °C), forging, sand-blasting and pickling (acid etching) steps until the final diameter was achieved. The chemical composition is listed in Table 1.

Cylindrical tensile specimens with a gage length of 25.4 mm and a gage diameter of 5.08 mm were machined from the as-received Zircaloy-2 rod. The tensile specimens were subsequently annealed at the Albany Research Center, Oregon, in evacuated quartz tubes for 0.5 h at 780 °C, in a vacuum of $10^{-1}$–$10^{-2}$ Pa. The average grain size of the annealed Zircaloy-2 was determined to be 7 μm in the transverse direction and 8 μm in the longitudinal (axial) direction using the average line-intercept method. Constant true-stress uniaxial creep tests were performed on the Zircaloy-2 specimens between 24–52 MPa and 500–600 °C in air. The creep tests were performed on a Satec dead weight creep-testing machine with a three-zone furnace, which maintained a constant temperature profile along the length of the specimen to within ±1 °C. Strain was measured in situ using a high-temperature Measuretron Series 4112 Linear Variable Capacitance Transducer (LVDT) extensometer with an accuracy of approximately 0.02%. Constant stress was maintained in all tests by incrementally removing weights from the load after every 1–2% strain. The creep samples were wrapped in titanium foil to help mitigate oxygen absorption. Two constant strain rate creep tests were performed to failure on cylindrical Zircaloy-2 specimens at a strain rate of $5 \times 10^{-5}\ s^{-1}$ and temperatures of 300 and 350 °C on an Instron 8521 servo-hydraulic tensile testing machine with collet-type grips and an ATS 3-zone furnace to evaluate the creep fracture behavior. Polishing of sectioned samples was performed using either ion etching or etch-attack polishing. Rough etch-attack polishing utilized a solution of 91% $H_2O$, 8% $HNO_3$, and 1% Hf with a slurry of 1-μm alumina powder. Final etch-attack polishing utilized a solution of 80% $H_2O$, 12% $HNO_3$, 8%

Table 1
Composition of the Zircaloy-2 utilized in this study

| | | | | | | | |
|---|---|---|---|---|---|---|---|
| Zr | 98.25 | Al | 29 | H | <3 | Nb | <50 |
| Cr | 0.10 | B | 0.3 | Hf | 52 | Pb | <25 |
| Fe | 0.19 | C | 133 | Mg | <10 | Si | 91 |
| Ni | 0.07 | Cd | <0.2 | Mn | <25 | Ti | 29 |
| O | 0.13 | Co | <10 | Mo | <10 | U | <1 |
| Sn | 1.26 | Cu | <25 | N | 32 | W | <50 |

Elements in the first column are reported in wt%, while all other elements are measured in ppm (as reported by Allegheny Wah Chang).

$H_2O_2$, and 0.5% Hf with a slurry of 0.05-μm alumina powder.

## 5. Results and discussion

### 5.1. Creep tests

The constant stress and constant strain rate creep data obtained in this study are compared to the literature data in Fig. 2. The Zircaloy-2 creep data were normalized by a self-diffusion coefficient with an activation energy, $Q$, of 270 kJ/mol and a (typical) pre-exponential, $D_0$, of $5 \times 10^{-4}$ m$^2$/s [36]. It is apparent from Fig. 2 that constant stress creep data measured in this study (samples Zr2-1, Zr2-6 and Zr2-7 in Fig. 2) fit within the range of data from the literature and are all within the five-power-law regime. The constant strain rate data (samples Zr2-11 and Zr2-15) were clearly in the power-law breakdown regime.[1] The failure time, failure strain, reduction of area and strain rate for specimens Zr2-11 and Zr2-15 (the only specimens tested to failure) are listed in Table 2.

The primary purpose of the creep and creep fracture tests performed during this study was to evaluate the failure mechanism controlling fracture of Zircaloy-2 under stresses (constant stress tests) or temperatures (constant strain rate tests) that are similar to the conditions during the dry storage of spent nuclear fuel. The fracture times measured for the two creep fracture tests on samples Zr2-11 and Zr2-15 performed during this study were not compared to the fracture times predicted by the theoretical failure models because steady-state creep was not achieved. The stress and strain rate values used to predict the failure time in the creep fracture models discussed above assume steady-state conditions. As will be discussed below, however, the condition of the material at and near the fracture surface allowed for a qualitative assessment of the fracture mechanism associated with failure under these conditions.

### 5.2. Creep cavitation

In order to evaluate whether cavitation occurred during creep of Zircaloy-2, two specimens that were tested into (Zr2-7, 52.25 MPa, 500 °C) and beyond[2] (Zr2-6, 48.19 MPa, 500 °C) the steady-state creep regime were sectioned both parallel and perpendicular to the applied stress. The specimens were polished and then ion etched before examination with an AmRay 20 keV scanning electron microscope (SEM) at Oregon State University. Ion etching was utilized to avoid any preferential etching effects (at precipitates, inclusions, etc.) sometimes associated with chemical etches. Some cavities observed in one specimen creep-tested for 27.8 h at 600 °C and 48.19 MPa (0.48 true strain) after grinding, polishing and ion etching are shown in Fig. 3. Upon examination of the gage sections of the creep specimens it was found that there was a certain level of cavitation present in the as-received specimens. This is consistent, although less pronounced, with what the authors have found to be true with as-received commercially pure zirconium [21]. Cavities such as the one shown in the left micrograph of Fig. 3 were unique to the gage sections of the creep-tested samples. The cavity in the left micrograph of Fig. 3 appears to consist of a coalescence of at least three smaller cavities. Qualitatively, it was quite apparent during the SEM examination that there was less evidence of cavitation in the grip sections of the specimens than in the gage sections. In order to quantify this difference, the cavity density in the gage section of the specimens was evaluated by counting the number of cavities parallel and perpendicular to the applied stress over an area of 0.15 mm$^2$, and comparing that to the cavity density in the respective orientations of the grip sections. The results of this examination are shown in Fig. 4.

It is interesting to note that, although the level of strain is quite different for Sample Zr2-6 than Sample Zr2-7, the number of cavities observed in the gage section of both samples appeared quite similar. The average cavity density in the gage section of the samples was clearly higher than in the grip sections of both samples. For reference, the fracture strain at 600 °C (Sample Zr2-6) was calculated to be

Table 2
Creep test results from the constant strain rate creep tests

| Sample | $T$ (°C) | $t_f$ (s) | $\varepsilon_f$ | RA (%) | $\dot{\varepsilon}$ (s$^{-1}$) |
|---|---|---|---|---|---|
| Zr2-11 | 300 | 7474 | 1.31 | 71.1 | $5 \times 10^{-5}$ |
| Zr2-15 | 350 | 6870 | 1.35 | 74.0 | $5 \times 10^{-5}$ |

[1] The constant strain rate creep tests did not reach steady state. The average stress and minimum strain rate are plotted in Fig. 2 to show the approximate location of the data relative to the three creep regimes.

[2] Steady-state creep was achieved with Sample Zr2-6, but the sample was not unloaded until tertiary creep had begun.

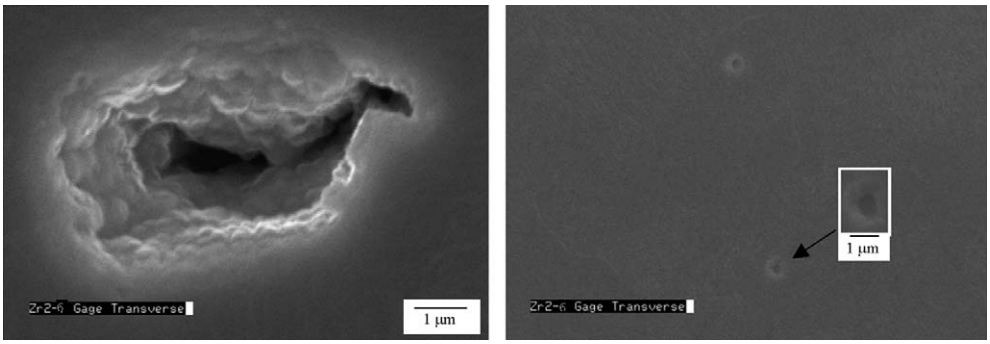


Fig. 3. SEM micrographs of Sample Zr2-6 gage section, transverse orientation, after 27.8 h at 600 °C and 48.19 MPa (0.48 true strain) (ground, polished and then ion etched). The applied stress is perpendicular to the page.

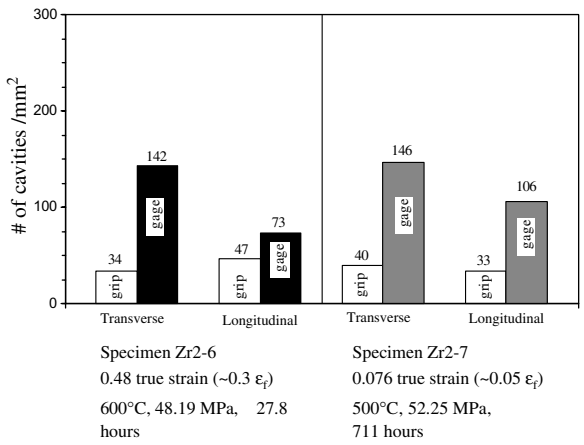


Fig. 4. Cavity density comparison between the grip section and the gage section in the transverse and longitudinal orientations of Samples Zr2-6 and Zr2-7 after ion etching.

approximately 1.6 based the fracture strains observed at 300 and 350 °C during the two constant strain rate tests performed in this study. Sample Zr2-6 was, therefore, tested to a strain that was approximately 30% of the failure strain (0.48 compared to 1.6). The fracture strain at 500 °C (Sample Zr2-7) was calculated to be approximately 1.5 based the fracture strains observed at 300 and 350 °C. Sample Zr2-7 was, therefore, tested to a strain that was approximately 5% of the failure strain (0.076 compared to 1.5). This indicates that the cavities likely nucleate in Zircaloy after even low strains and long before tertiary creep (test Zr2-7 was stopped in the steady-state, or secondary, creep regime). The fact that the observed cavity densities were similar in Samples Zr2-6 and Zr2-7 for very different levels of strain *may* suggest that nucleation occurs early in the creep life, followed by a cavity growth process. This observation is somewhat tenuous, however, since the two tests were performed at different temperatures. An analysis of the cavity nucleation rate and cavity growth rate in these samples was beyond the scope of this study.

In order to determine whether the difference in the cavity density between the grip and the gage sections of the samples was statistically significant, a binary responses statistical analysis was performed. A binary responses technique was chosen because the cavity density was low enough in all cases (grip and gage) that there was rarely any more than 1 cavity in each 1500-μm$^2$ SEM micrograph used to count cavities. For this analysis, 100 micrographs were examined from each orientation indicated in Fig. 4 and assigned either a 'yes' or a 'no'. 'Yes' indicated that there was at least one cavity present in the micrograph. 'No' indicated that there were no cavities detected in the micrograph. The 'odds' of detecting a cavity in any given 1500-μm$^2$ micrograph was calculated by taking the proportion of the number of 'yes' micrographs to the number of 'no' micrographs. The results of this statistical analysis are summarized in Table 3.

There was strong statistical evidence that the difference between the cavity density in the grip and gage sections of Samples Zr2-6 and Zr2-7 (shown in Fig. 4) was due to creep deformation. As can be observed in Table 3, the estimated odds ratio

Table 3
Statistical results from the binary variables analysis of the odds ratios of the cavity count data

| Sample | One-sided *p*-value | Odds ratio | 95% Confidence interval of the odds ratio |
|---|---|---|---|
| Zr2-6 | 0.0001 | 3.0 | 1.5–6.0 |
| Zr2-7 | 0.000002 | 4.2 | 1.9–9.0 |

for Sample Zr2-6 was 3.0. This indicates that the odds of finding a cavity in the gage section of a Zircaloy-2 specimen tested under the conditions used to test Sample Zr2-6 are estimated to be 3.0 times as large as the odds of finding a cavity in the grip sections of the same sample. Similarly, the odds of finding a cavity in the gage section of a Zircaloy-2 specimen tested under the conditions used to test Sample Zr2-7 are estimated to be 4.2 times as large as the odds of finding a cavity in the grip sections of the same sample.

The cavity densities in the gage sections of Samples Zr2-6 and Zr2-7 are clearly higher than the grip sections of the samples. The source of the cavities in the gage sections of Samples Zr2-6 and Zr2-7 is unclear because cavities were also observed in the grip sections of both samples. The cavities in the gage sections either nucleated and grew during creep, or were pre-existing in the material after the manufacturing process and simply grew to a detectable size only after the application of a creep stress.

### 5.3. Creep fracture

After testing samples Zr2-11 and Zr2-15 to failure, the fracture surfaces of both samples were examined with the SEM. The fracture surface of one sample is shown in Fig. 5. The fracture surface in the upper left micrograph of Fig. 5 is outlined by white dashed lines. (The material outside the white dashed lines in this micrograph is the shoulder and grip of the specimen.)

The fracture surfaces shown in Fig. 5 indicate a typical ductile fracture with extensive cavitation. The high magnification image shown at the bottom right of Fig. 5 shows a distribution of various-size cavities over the entire fracture surface. The fractured specimens were sectioned both transverse and longitudinal orientations before mounting and polishing. SEM images taken from longitudinal orientation of Samples Zr2-11 near the fracture surface are illustrated in Figs. 6 and 7. As can be observed in Figs. 6 and 7, there was extensive cavitation near

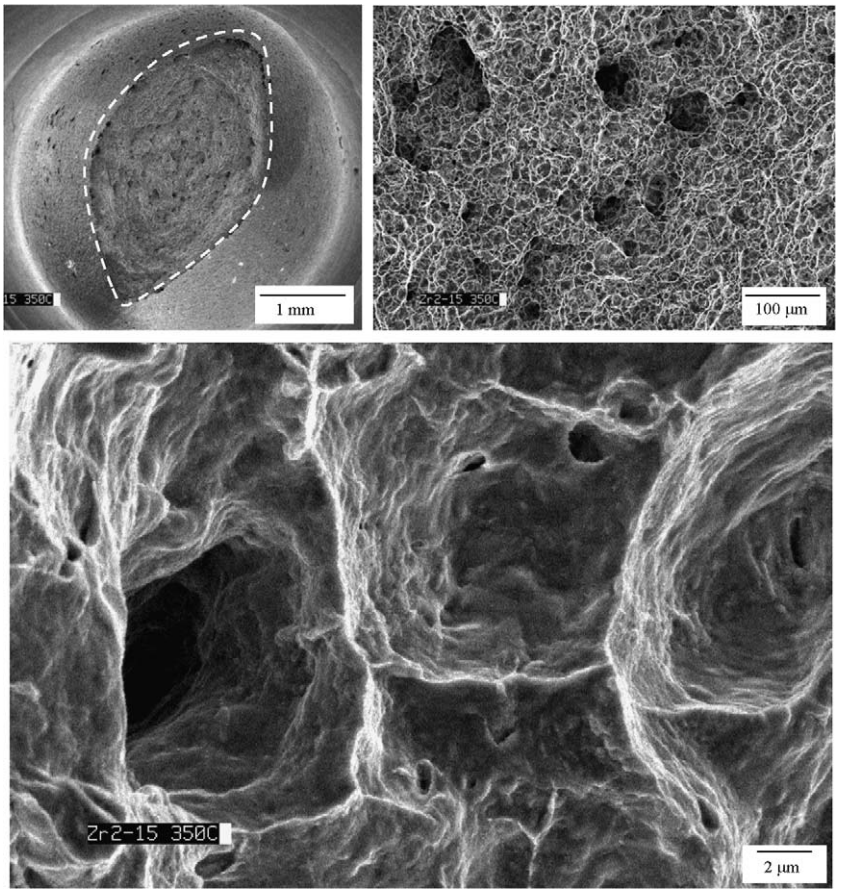


Fig. 5. SEM images of Sample Zr2-15 fracture surface after testing to failure at 350 °C and a constant strain rate of $5 \times 10^{-5}$ $s^{-1}$.

the fracture surface. The small light areas in the micrographs appear to be cavities that 'opened up' near the end of the etch-attack polishing procedure such that the material at the edges of the cavities flared out (see, for example, the two micrographs at the bottom of Fig. 6). Using the same technique of counting cavities described above (over an area of approximately 0.04 $mm^2$ in this case), it was determined that the cavity density near the fracture surface was approximately 2750 cavities/$mm^2$. The true strain at this location was approximately 1.31. When comparing this cavity density to the cavity densities measured for Samples Zr2-6 and Zr2-7, it should be kept in mind that the cavity density (measured as the number of cavity per $mm^2$) here is the result of a combination of void nucleation and void coalescence. Cavity nucleation increases the cavity density while cavity coalescence (interlinkage of cavities) decreases the cavity density by decreasing the number of cavities. The fact that the cavity density near fracture is so much higher than the cavity density observed in Samples Zr2-6 and Zr2-7 after 0.48 and 0.076 strain, respectively, indicates that cavity nucleation occurred at some point during creep deformation and that not all the cavities were simply present in the as-received material.

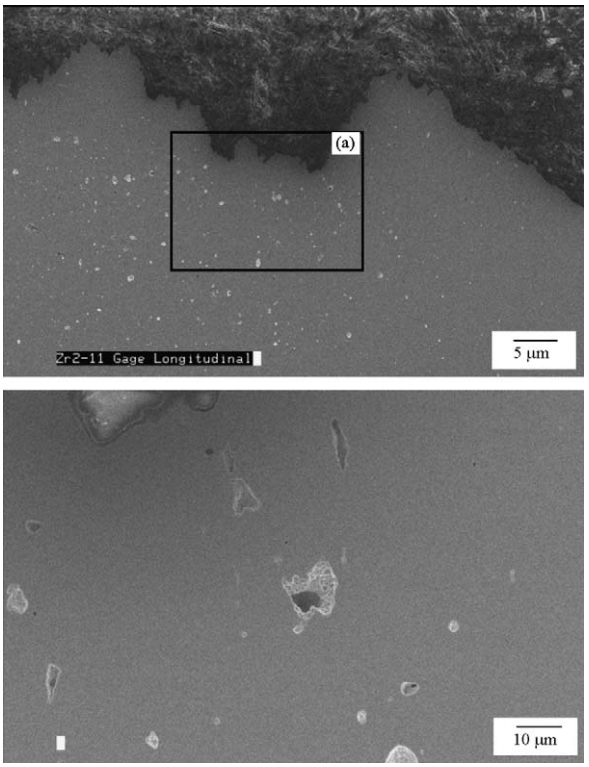


Fig. 6. Sample Zr2-11 gage section, longitudinal orientation, near the fracture surface.

The upper left micrograph in Fig. 7 shows a higher magnification micrograph from the region outlined with a black box in Fig. 6. One of the larger cavities in this region is illustrated in more detail in the remaining three micrographs in Fig. 7. The shape of the perimeter of the cavity and the cavities

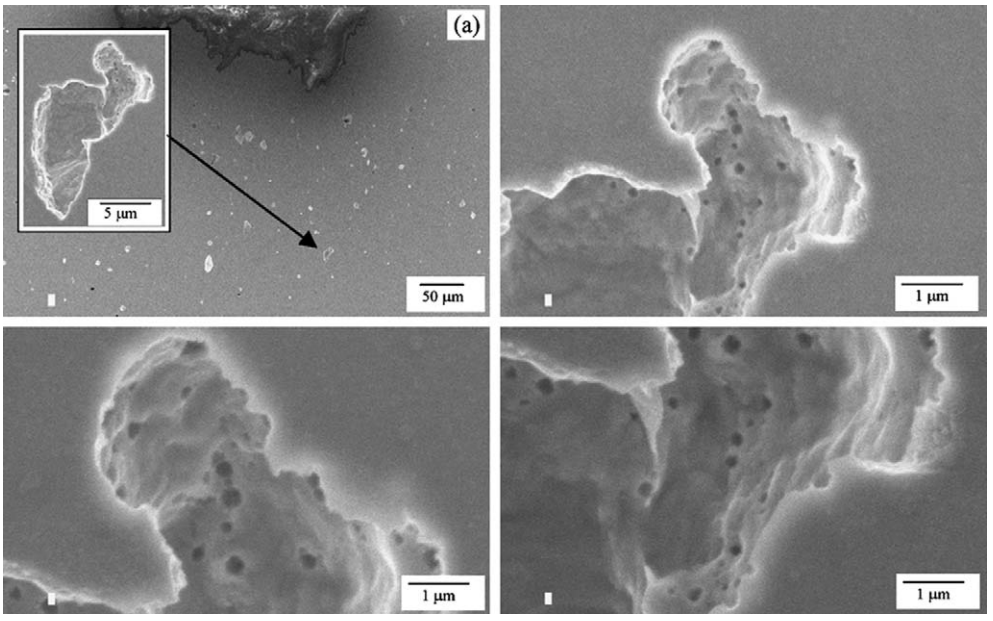


Fig. 7. Higher magnification of region (a) in Fig. 6 (Sample Zr2-11 gage section, longitudinal orientation).

appearing on the interior surfaces of the cavity suggest that this is an interlinkage of cavities. This indicates that damage in Zircaloy-2 under these conditions is consistent with a cavity growth and interlinkage model.

## 6. Conclusions

Constrained cavity growth appears to be a more relevant failure model for predicting the lifetime of spent nuclear fuel while stored in interim dry storage than a classical unconstrained diffusion controlled cavity growth mechanism. Constrained cavity growth can account for the Monkman–Grant relationship, which has been shown to be valid for Zircaloy, and appears to be relevant to most SNF dry storage conditions.

An extensive examination of creep-deformed samples in an SEM suggests that Zircaloy-2 is susceptible to creep cavity formation and growth, and fails as a result of cavitation damage. Extensive cavitation damage was observed before failure in two Zircaloy-2 specimens tested at a constant strain rate at temperatures of 300 °C and 350 °C. The high cavity densities observed near creep fracture after these constant strain rate tests suggest that cavity nucleation and growth occurred during creep deformation in these tests. The cavity density in the gage sections of two creep specimens tested at constant true stress to strains of 0.076 and 0.48 at temperatures of 500 and 600 °C, respectively, were statistically significantly higher than in the grip sections of those samples. The extent to which creep cavities nucleated during creep deformation in these specimens is unclear because some level of cavitation was also observed in the as-received Zircaloy-2 and in the grip sections of the creep-tested specimens. It is unclear whether these cavities actually nucleated during the creep process, or were present in the as-received material and just grew to detectable sizes after being subjected to elevated stresses and temperatures. The dramatic increase in cavity density observed near the fracture surface of the constant strain rate creep tests suggests, however, that at least some cavity nucleation occurs during creep deformation of Zircaloy-2.

## Acknowledgements

The views expressed are solely those of the authors and no official support or endorsement of this article by the Defense Nuclear Facilities Safety Board, the Department of Energy, or the federal government is intended or should be inferred. This work was performed under the auspices of the US Department of Energy (DOE) by Lawrence Livermore National Laboratory (LLNL) under Contract W-7405-ENG-48, and a subcontract from LLNL to the University of California, San Diego, under contract B345708 515. The financial support from the DOE National Spent Nuclear Fuel Program and Office of Spent Fuel Management (EM-67), the Materials Research Institute at Lawrence Livermore National Laboratory, and Sigma Xi is greatly appreciated.

## References

[1] US Nuclear Regulatory Commission, Final Report, NUREG-1536, January 1997.
[2] US Nuclear Regulatory Commission, Spent Fuel Project Office Interim Staff Guidance – 11, 13 May 1999.
[3] US Nuclear Regulatory Commission, Spent Fuel Project Office Interim Staff Guidance – 11, Revision 2, 30 July 2002.
[4] US Nuclear Regulatory Commission, Spent Fuel Project Office Interim Staff Guidance – 11, Revision 3, 17 November 2003.
[5] C. Pescatore, M.G. Cowgill, Final Report, Brookhaven National Laboratory, EPRI TR-103949, May 1994.
[6] P.J. Henningson, J.T. Willse, B. Cox, M.G. Bale, K.L. Murty, W.A. Pavinich, Framatome Technologies Report, 51-1267509-00, December 1998.
[7] R.L. Keusseyan, C.P. Hu, C.Y. Li, J. Nucl. Mater. 80 (1979) 390.
[8] D. Hull, D.E. Rimmer, Philos. Mag. 4 (1959) 673.
[9] R. Raj, M.F. Ashby, Acta Metall. 23 (1975) 653.
[10] M.V. Speight, W. Beere, Met. Sci. 9 (1975) 190.
[11] M.W. Schwartz, M.C. Witte, Lawrence Livermore National Laboratory, UCID-21181, September 1987.
[12] I.S. Levy, B.A. Chin, E.P. Simonen, C.E. Beyer, E.R. Gilbert, A.B. Johnson Jr., Pacific Northwest Laboratory, PNL-6189, May 1987.
[13] R. Raj, Acta Metall. 26 (1978) 341.
[14] L.-E. Svensson, G.L. Dunlop, Met. Sci. 16 (1982) 57.
[15] M.D. Hanna, G.W. Greenwood, Acta Metall. 30 (1982) 719.
[16] J.M. Mintz, A.K. Mukherjee, Metall. Trans. A 19A (1988) 821.
[17] B.D. Clay, G.B. Redding, J. Brit. Nucl. Energy Soc. 15 (1976) 253.
[18] M.E. Kassner, M.-T. Perez-Prado, Fundamental of Creep in Metals and Alloys, Elsevier, 2006, p. 1.
[19] H. Riedel, Fracture at High Temperatures, Materials Research and Engineering, Springer-Verlag, 1987.
[20] T.A. Hayes, M.E. Kassner, Metall. Mater. Trans., in press.
[21] T.A. Hayes, PhD Dissertation, University of California, San Diego, 2004.
[22] A. Wolfenden, K. Farrell, Scripta Metall. 6 (1972) 127.
[23] G.J.C. Carpenter, Radiat. Eff. 19 (1973) 189.
[24] D. Lee, E.F. Kock, R.B. Adamson, W.L. Bell, in: Zirconium in Nuclear ApplicationsASTM STP 551, American Society for Testing and Materials, Philadelphia, 1974, p. 215.

[25] A. Riley, P.J. Grundy, Phys. Status Solidi A 14 (1972) 239.
[26] M. Yoo, in: Zirconium in Nuclear ApplicationsASTM STP 551, American Society for Testing and Materials, Philadelphia, 1974, p. 292.
[27] D.O. Northwood, At. Energy Rev. 15 (1977) 547.
[28] M. Hadji-Mirzai, K.C. Russell, J. Nucl. Mater. 92 (1980) 229.
[29] M. Griffiths, J. Nucl. Mater. 159 (1988) 190.
[30] M. Griffiths, R.W. Gilbert, C.E. Coleman, J. Nucl. Mater. 159 (1988) 405.
[31] M. Griffiths, R.C. Styles, C.H. Woo, F. Phillipp, W. Frank, J. Nucl. Mater. 208 (1994) 324.
[32] M. Griffiths, D. Gilbon, C. Regnard, C. Lemaignan, J. Nucl. Mater. 205 (1993) 273.
[33] A. Jostsons, P.M. Kelly, R.G. Blake, K. Farrell, in: Effects of Radiation on Structural MaterialsASTM STP 683, American Society for Testing and Materials, Philadelphia, 1979, p. 46.
[34] M. Mayuzumi, T. Onchi, J. Nucl. Mater. 175 (1990) 135.
[35] K.L. Murty, Y. Zhou, B. Devarajan, in: R.S. Mishra, J.C. Earthman, S.V. Raj (Eds.), Creep Deformation: Fundamentals and Applications, TMS, 2002, p. 31.
[36] T.A. Hayes, M.E. Kassner, R.S. Rosen, Metall. Mater. Trans. 33A (2002) 337.